A Quasi-optical THz Imaging System Using a One-port Vector Netowrk Analyser

Zimo Zhao, Michael E Farage, Yi Yi, Chong Li*
James Watt School of Engineering
University of Glasgow
Glasgow, UK
*Chong.Li@glasgow.ac.uk

***Abstract*—In this paper we demonstrate a simple single-pixel quasi-optical imaging setup with a one-port 140 GHz-220 GHz vector network analyser (VNA), a pyramidal horn antenna, a plano-convex lens and an X-Y translation stage. By placing an object at the focal plane of the lens and measuring its one-port S-parameters while scanning the object fixed onto the X-Y translation stage, 2D images of the object are constructed using S-parameter magnitude and phase information. The results show that the phase constructed image is better than magnitude constructed image in some cases. This finding indicates that VNA can be useful in THz imaging as it provides more information from the perspective of phase which can be used to enhance imaging.**

Keywords—THz, VNA, quasi-optical, S-parameter

I. Introduction

Terahertz is part of electromagnetic spectrum covering 0.1 THz-3 THz and has a wavelength between 3 mm-0.1 mm. As this section of spectrum sits between infrared and microwave, it thus processes characteristics of both bands. Many dielectric materials and fabrics are transmissive to THz and sub-millimeter wave frequencies, which provide convenience to detect covered objects [1]. In addition, many substances have their characteristic absorptions lines lie in this frequency band. Benefiting from these properties, the THz window becomes attractive in many applications including spectroscopy [2-3] and security imaging [4-5]. Over the past three decades, many different imaging techniques have been developed and their applications have been extended into many practical applications including detection of concealed weapons [6], quality control in pharmaceutics [7], medical diagnosis [8-9] and many more.

Amongst the THz imaging systems, time domain spectroscopy (TDS) is one of the most widely used [10-11]. TDS has the advantages of simple setup and relatively low cost. However, TDS also faces low signal to noise ratio due to low source power. Electronics-based solutions also show strong competition in both active [12] and passive [13] imaging for security screening. A VNA setup has recently been demonstrated for analysis of water concentration [14-15] and contamination in plants [16]. In this paper, we will demonstrate a quasi-optical setup with a 140 GHz-220 GHz VNA for imaging applications. By taking advantage of VNA's wide frequency tuning range and capability of exhibiting both magnitude and phase information, we managed to construct phase and magnitude based 2D images of an object at various frequencies. Further investigation shows that the images constructed using phase information could be better than those based on magnitude. This finding could potentially lead to a better development of imaging systems and applications.

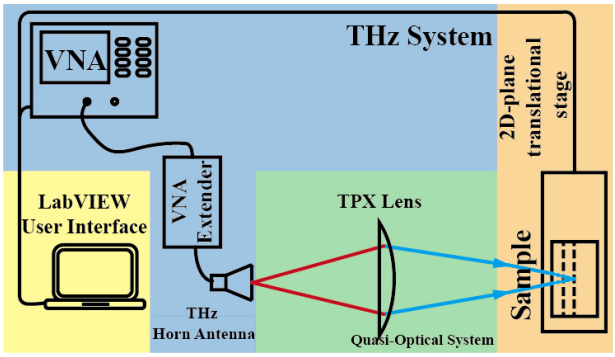

(a)

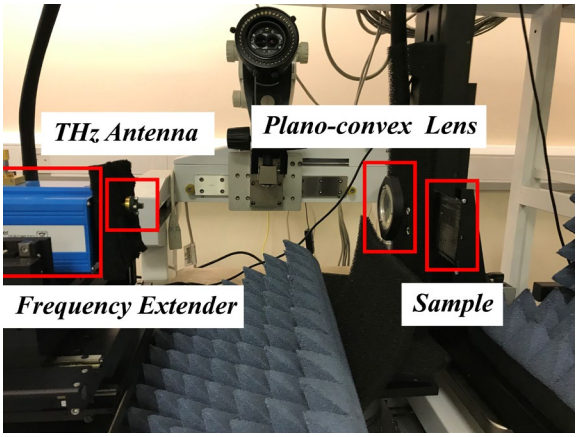

(b)

Fig. 1. (a) Schematic illustration and (b) the actual setup of VNA-based reflection mode quasi-optical imaging system.

The rest of this paper is organised as follows. Section II will introduce the imaging system and Section III will discuss and analyse the results. The main results in this paper are concluded in Section IV.

II. The Imaging System

A VNA-based reflection-mode quasi-optical THz imaging setup is shown in Fig. 1. It consists of a one-port 140 GHz-220 GHz VNA (Keysight E8364B+OML V05VNA2-T/R frequency extender head), a 140 GHz-220 GHz 20 dB pyramidal horn antenna, a plano-convex TPX lens and a X-Y imaging plane formed by two linear translation stages (LTS) with integrated controllers (Thorlabs LTS300). The diameter of the TPX lens is 35 mm with a focal length of 30 mm at 180 GHz. To reduce system noise during measurements, the VNA was calibrated to the end of waveguide port before mounting pyramidal THz horn antenna. The translation stage has a minimum movement accuracy of 5 um. Absorbing materials were used to reduce reflections. A LabVIEW program has

Table I. Measurement setup parameters

Symbol	Parameter	Value
f_{min}	Start Frequency	140 *GHz*
f_{max}	Stop Frequency	220 *GHz*
B	Bandwidth	80 *GHz*
f_{IF}	Intermediate Frequency bandwidth	1 *kHz*
N	Sweep points	11
L	Scanned area length	30 *mm*
W	Scanned area width	12 *mm*
Δx	Scan step on length	0.5 *mm*
Δy	Scan step on width	0.5 *mm*

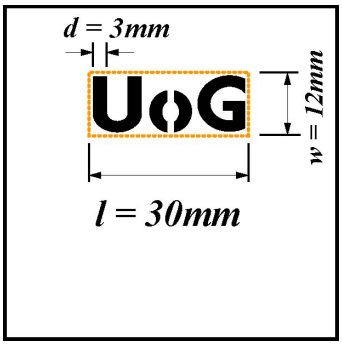

Fig. 2. Illustration of the imaging object used in this experiment.

been developed for system control, data acquisition and image construction. Fig. 2 shows the imaging object used in this experiment. It is a 2-mm thick aluminium plate with etched-through letters of "UoG". The gap has a nominal width of 2 mm. Some absorbing materials were also placed at the back of the sample to reduced double reflection. Table I summarises other parameters of the setup.

With reference to Fig. 1, the continuous wave (CW) signal transmitted from the horn antenna propagates to the TPX lens. Because the TPX lens is placed at the far-field distance of the horn antenna, the field incident on the lens is considered a plane wave. Therefore, the field propagating from the lens will then be converged to the focal point at the object plane. Due to the reciprocal nature of the configuration, fields reflected by the sample will be transformed to a plane wave by the lens and received by the horn antenna. The diameter of the focal spot varies with frequency due to the lens aberration and phase centre movement of the horn antenna. Thus, an image can be formed by movement of the X-Y translation stage, which moves in the focal plane. As the LTS is mechanically scanned, the power incident on the sample will be reflected or absorbed depending on the features of the object. Thus, the single port VNA configuration will only measure the reflected power. Therefore, 2D images of the object can be constructed by analysing the magnitude and phase content of the measured reflection coefficient (S_{11}) as the LTS scans the image plane. In the following section we will demonstrate how this setup is used to construct an image of a simple object made of a piece of aluminium plate with through patterns, as shown in Fig. 2.

III. Measurement Results and Discussion

To demonstrate the imaging setup, a region of 30 mm by 12 mm on the object, as shown by the dotted area of Fig. 2, was scanned. The scan step was set to be Δx=Δy=0.5 mm, which results in a total of 1525 points. The complex reflection

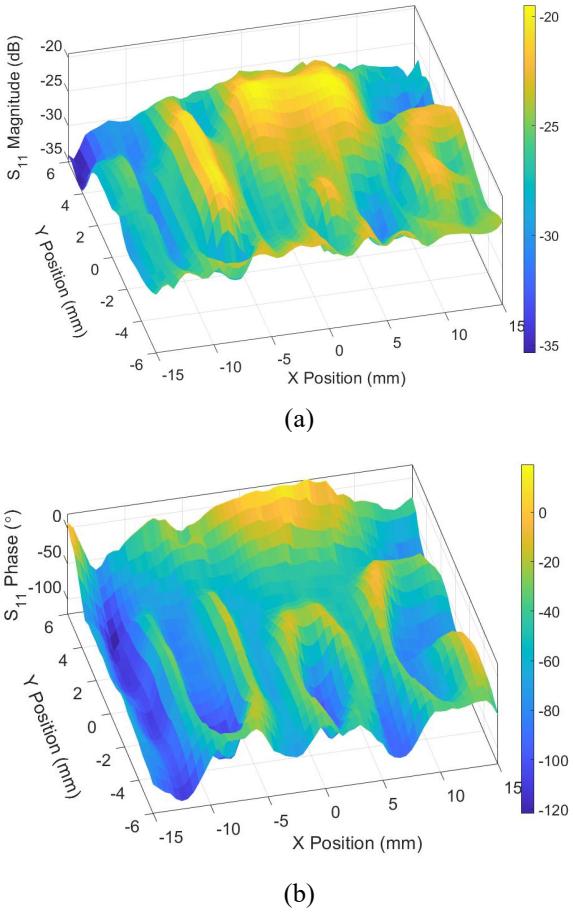

Fig. 3. (a) Magnitude image and (b) phase image constructed using the VNA-based reflection mode quasi-optical imaging setup.

coefficient between 140 GHz and 220 GHz with 11 points were measured at each point. Using the magnitude and phase of the measured S_{11}, we construct reflection-mode images of the object at 160 GHz as shown in Fig. 3. The object has a flat surface everywhere except the three letters. For the metallic sample shown in Fig. 2, the S_{11} magnitude is expected to be larger when unetched areas are imaged because significantly more power will be reflected by aluminium surface whereas most of the power transmitted through the etched features is absorbed by the material behind the sample. However, this is not true for Fig. 3a in which the object is poorly resolved. Because the 0.5 mm sample thickness is comparable in size to the wavelength of the incident fields, scattering occurs when the side walls of the etched features lie near or within the focal spot of the TPX lens. According to Huygens–Fresnel principle, the scattered waves will be reflected to the lens and detected

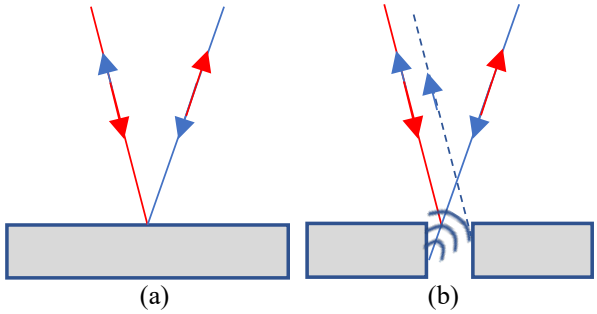

Fig. 4. Illustrations of (a) normal reflection from a flat aluminium sample. (b) reflections occur at a gap due to refraction.

by the antenna and VNA detector, thus the boundaries between the aluminium and air are indistinguishable. This is illustrated in Fig. 4. The dashed blue line in Fig. 4b corresponds to the diffracted wave generated due to Huygens–Fresnel principle. Additionally, VNA characteristics such as output power and receiver dynamic range will further degrade the distinction between etched and unetched regions when coupled with THz propagation losses.

In comparison, Fig. 3b shows the image using just S_{11} phase information is much clearer than that constructed using only S_{11} magnitude. This is because the phase difference of the reflected field due to refraction is different from that of normal reflection at the surface as shown in Fig. 4a. With this information greater details such as material thickness can be calculated to a certain degree. The relationship between phase difference and material thickness can be described as:

$$z = \frac{D \cdot \lambda}{2 \cdot 360} \quad (1)$$

where D is the phase difference (in degrees) between the flat surface and the refraction centre, λ is wavelength (in m). To verify this, we choose the Y=0 cut (Fig. 5a) and plot the thickness calculated using (1) in Fig. 5b. One can see the S_{11} phase converted thickness does reflect difference between the surface and the gap but there is discrepancy between the actual

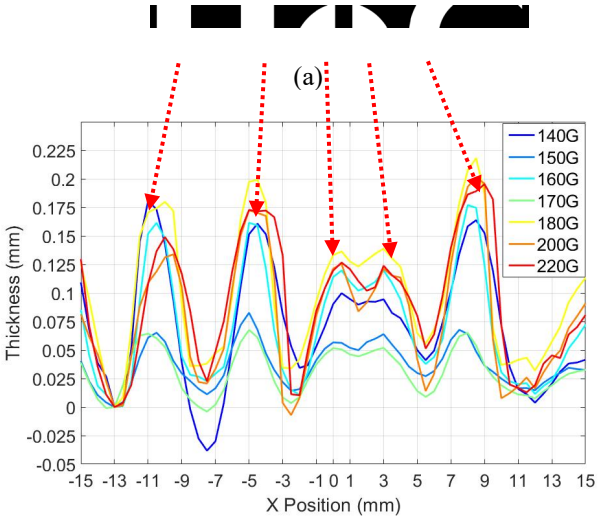

Fig. 5. Thickness of the object sample at the cross-section of Y=0. (a) shows the location of the real sample (b) the corresponding thickness.

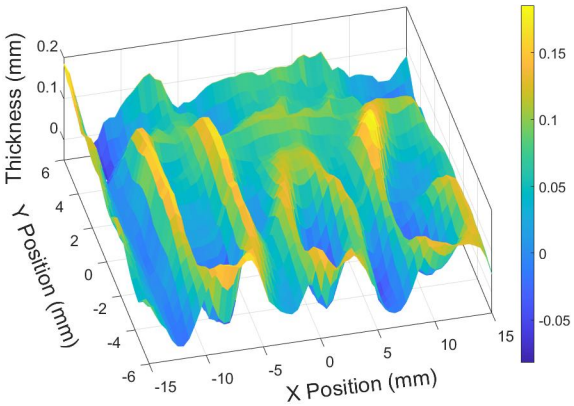

Fig. 6. Tilt correct image of Fig. 3b.

depth and measured depth. This is perhaps due to gap width and beam angle and warrants further investigation.

Apart from gap depth, the S_{11} phase information is also able to correct sample tilt. Assuming the sample surface is perfectly flat and there is no tilt, the phase at any scanning line without a gap should be the same; However, this is difficult to achieve in reality. In this experiment, significant efforts were made to ensure the object was perpendicular to the incident field, we still can see non-uniform phase distribution from Fig. 3b for example when X=-13 mm. Since phase at the two ends of the sample differs, we can use this information to correct the tilt. Fig. 6 shows the corrected image of Fig. 3b.

The imaging system can be further improved by adding an additional axial axis for 3-D scans. Three-axis scans will enable the system to reveal greater details of the inner structure of the sample layer-by-layer. Therefore, complex structures or a curved surface can be imaged. Also, other advanced optical systems, like confocal optical lenses system, can be placed between VNA ports to improve the quality of images.

IV. Conclusion

In this paper, we presented a simple single-pixel quasi-optical imaging system. The system consists of a 140 GHz-220 GHz VNA, a pyramidal horn antenna, a plano-convex lens and an X-Y translation stage. When an object was scanned on the focal plane of the lens, complex one-port reflection coefficients S_{11} at each point were obtained. We compared the 2D images of the object constructed using both magnitude and phase of the S-parameters and conclude that the phase constructed image could be better in some cases. This is because refraction at small aperture blur the boundaries for magnitude constructed images. This finding indicates that VNA can be very useful in THz imaging as it provides more insights of phase information which can be used to enhance imaging quality.

References

[1] P. Siegel, “Terahertz technology,” IEEE Transactions on Microwave Theory and Techniques, vol. 50, pp. 910–928, Mar 2002.

[2] B. M. Fischer, H. Helm, and P. U. Jepsen, “Chemical recognition with broadband THz spectroscopy,” Proceedings of the IEEE, vol. 95, pp. 1592–1604, Aug 2007.

[3] N. Laman, S. S. Harsha, D. Grischkowsky, and J. S. Melinger, “Highresolution waveguide THz spectroscopy of biological molecules,” Biophysical Journal, vol. 94, pp. 1010–1020, Feb 2008.

[4] J. F. Federici, B. Schulkin, F. Huang, D. Gary, R. Barat, F. Oliveira, and D. Zimdars, “THz imaging and sensing for security applications—explosives, weapons and drugs,” Semiconductor Science and Technology, vol. 20, pp. S266–S280, Jun 2005.

[5] Q. Song, Y. Zhao, A. RedoSanchez, C. Zhang, and X. Liu, “Fast continuous terahertz wave imaging system for security,” Optics Communications, vol. 282, pp. 2019–2022, May 2009.

[6] J. F. Federici, D. Gary, R. Barat, and D. Zimdars, “THz standoff detection and imaging of explosives and weapons (invited paper),” in Optics and Photonics in Global Homeland Security (T. T. Saito, ed.), SPIE, May 2005.

[7] K. E. Peiponen, P. Silfsten, J. Pajander, and J. Ketolainen, “Broadening of a THz pulse as a measure of the porosity of pharmaceutical tablets,” International Journal of Pharmaceutics, vol. 447, pp. 7–11, Apr 2013.

[8] S. J. Oh, J. Kang, I. Maeng, J. S. Suh, Y. M. Huh, S. Haam, and J. H. Son, “Nanoparticleenabled terahertz imaging for cancer diagnosis,” Optics Express, vol. 17, p. 3469, Feb 2009.

[9] M. A. Brun, F. Formanek, A. Yasuda, M. Sekine, N. Ando, and Y. Eishii, “Terahertz imaging applied to cancer diagnosis,” Physics in Medicine and Biology, vol. 55, pp. 4615–4623, Jul 2010.

[10] W. Withayachumnankul and M. Naftaly, “Fundamentals of measurement in terahertz timedomain spectroscopy,” Journal of Infrared, Millimeter, and Terahertz Waves, vol. 35, pp. 610– 637, Dec 2013.

[11] M. Hangyo, M. Tani, and T. Nagashima, “Terahertz timedomain spectroscopy of solids: A review,” International Journal of Infrared and Millimeter Waves, vol. 26, pp. 1661–1690, Nov 2005.

[12] F. Friederich, W. von Spiegel, M. Bauer, F. Meng, M. D. Thomson, S. Boppel, A. Lisauskas, B. Hils, V. Krozer, A. Keil, T. Loffler, R. Henneberger, A. K. Huhn, G. Spickermann, P. H. Bolivar, and H. G. Roskos, “THz active imaging systems with realtime capabilities,” IEEE Transactions on Terahertz Science and Technology, vol. 1, pp. 183–200, Sep 2011.

[13] M. Aoki, S. R. Tripathi, M. Takeda, and N. Hiromoto, “Passive imaging and emissivity measurement with a 4k-cryocooled terahertz photoconductive detector,” IEICE Electronics Express, vol. 9, no. 5, pp. 333–338, 2012.

[14] A. Zahid, K. Yang, H. Heidari, C. Li, M. A. Imran, A. Alomainy, and Q. H. Abbasi, “Terahertz characterisation of living plant leaves for quality of life assessment applications,” in 2018 Baltic URSI Symposium (URSI), IEEE, May 2018.

[15] A. Ren, A. Zahid, D. Fan, M. A. Imran, A. Alomainy, and Q. H. Abbasi, “Establishing a noveltechnique for the detection of water contamination using terahertz waves,” in 2019 IEEE MTT-S International Wireless Symposium (IWS), IEEE, May 2019.

[16] A. Ren, A. Zahid, M. A. Imran, A. Alomainy, and Q. H. Abbasi, “Introducing a novel techniqueof detecting fruits contaminations using terahertz sensing,” in 2019 International Workshop on Antenna Technology (iWAT), IEEE, Mar 2019.